# SHEAR-DRIVEN FLUSHING OF MICRO-TIDAL MARINAS

Enda Murphy[1], Mathieu Deiber[1] and Sylvain Perrin[2]

Flushing or residence times are typically used as a first step in assessing water quality in marinas, harbours and coastal basins. Recent publications have offered guidance in relation to optimal marina basin and entrance geometries to help achieve rapid renewal. However, these guidelines have been developed for the particular case where water exchange is strongly tide-driven and are not widely applicable, particularly in micro-tidal regions. Where water renewal rates are dominated by shear-driven circulation and lateral transfer of momentum at the interface between the marina and the adjacent water body (i.e. a mixing layer), there is a strong analogy to groyne fields and other cases involving flows containing quasi-stagnant peripheral areas (dead zones). A series of numerical hydrodynamic models, developed in the TELEMAC system, were used to investigate the potential for the dead zone model of water exchange to provide a better means to guide optimization of basin and entrance geometry under such conditions. Real-world marina case studies were used to identify any constraints affecting the practical implementation of such an approach. The numerical model results demonstrate particular conditions under which the dead zone model of water exchange can be used effectively to optimize marina basin and entrance geometry.

*Keywords: flushing; residence time; marina; water quality; dead zone; water renewal; water exchange*

## INTRODUCTION

Flushing or residence times have historically been used to provide an indication of potential water quality in marinas, harbours and coastal basins (Nielsen and McCowan 1994; USEPA 1985; Fischer et al. 1979). Recent publications have offered guidance in relation to optimal basin geometries (e.g. plan form factor, aspect ratio, tidal prism ratio, curvature, relative entrance area) to help achieve rapid renewal (Cox et al. 2008; Barber and Wearing 2002; USEPA 2001). However, these guidelines have been developed for the particular case where water exchange is strongly tide-driven and are not widely applicable, particularly in micro-tidal regions[3]. Since the majority of the world's coastal waters are micro-tidal (p. 176, Rafferty 2012), including the Mediterranean, the Baltic, the Persian / Arabian Gulf, the Red Sea and the Gulf of Mexico, there is significant incentive to broaden the applicability of these guidelines.

For micro-tidal marinas, assumptions that typically form the basis for tidal prism models of water exchange (Monsen et al. 2002) do not hold. Under these conditions and where meteorological forcing is relatively weak, water exchange is often dominated by shear-driven circulation and lateral transfer of momentum at the interface between the marina and the adjacent water body (i.e. a mixing layer). This exchange mechanism is analogous to riverine groyne fields and other situations where the flow field contains quasi-stagnant peripheral areas (dead zones). In these cases, dead-zone models for mass transport may present a better alternative to guide optimization of basin and entrance geometry.

In this paper, we extend previous work (Murphy and Walker 2011) aimed at investigating the applicability of dead-zone models of water exchange, traditionally used to evaluate mass transport in rivers and groyne fields, to micro-tidal marinas.

## DEAD-ZONE MIXING PROCESSES AND MODEL FOR WATER EXCHANGE

The effect of quasi-stagnant, or "dead" zones on water exchange and mass transport in rivers has been the subject of considerable research over the past four decades (Weitbrecht et al. 2008; Harvey et al. 2005; van Mazijk and Veling 2004; Schmid 2002; Atkinson and Davis 2000; Davis et al. 2000; Worman 2000; Harvey et al. 1996; Chikwendu and Ojiakor 1985; Valentine and Wood 1977). Dead zones, which are defined by Purnama (1988) as local areas of the flow cross section with relatively still water, or no net downstream velocity, are created in rivers by the presence of meanders (Seo and Cheong 2001), natural or manmade peripheral embayments (including marinas) (Weitbrecht et al. 2008), groyne fields (Weitbrecht et al. 2004; Weitbrecht et al. 2003), vegetated zones (Nepf et al. 2007; Ghisalberti and Nepf 2005; Harvey et al. 2005), hyporheic zones (Worman 2000), pools and riffles (Harvey et al. 1996; Bencala and Walters 1983).

---

[1] Sogreah Gulf – Artelia Group, Dubai, United Arab Emirates.
[2] Sogreah Grenoble – Artelia Group, Grenoble, France.

[3] Although the term "micro-tidal" is typically used to refer strictly to locations where tidal ranges are less than 2m (Pugh 1987), it is used here in a more general sense to refer to locations where the tidal range is simply "small".

Dead zones on the sides of channels result in shear flow at the interface with the main channel and an associated inflection point in the streamwise velocity profile. The latter is a characteristic of mixing layers, commonly observed in terrestrial (Raupach et al. 1996) and aquatic vegetated flows (Ghisalberti and Nepf 2002), and is a prerequisite criterion for instability (p. 499, Kundu and Cohen 2004). Mixing layers are susceptible to Kelvin-Helmholtz instability, such that transport across the layer is typically dominated by large scale vortex structures (Weitbrecht et al. 2008; Ghisalberti and Nepf 2002). The formation of vortices and the efficiency of exchange between the dead zone and the main channel, which are separated by the mixing layer, are subject to local flow conditions and the geometry of the dead zones (Weitbrecht et al. 2008; Ghisalberti and Nepf 2005; Valentine and Wood 1977; Riviere et al. 2010).

Most dead zone models consider exchange between stagnant zones and the main stream to be well represented by a first order process (Weitbrecht et al. 2008; Davis and Atkinson 2000; Chikwendu and Ojiakor 1985; Valentine and Wood 1977):

$$\frac{\partial C}{\partial t} = b\left(C - C_S\right) \tag{1}$$

where $C$ and $C_S$ are the concentrations of a conservative solute in the dead zone and main stream, respectively, $t$ is time, and $b$ is an exchange coefficient with dimensions $T^{-1}$. For a well-mixed dead zone (i.e. uniform concentrations throughout), the inverse of the exchange coefficient provides a measure of the time scale for water renewal within the dead zone, commonly referred to as the mean residence time, $T_R$. For an ideal (plane) mixing layer (Raupach et al. 1996), the exchange coefficient is known to be a function of the difference between the net streamwise velocity in the main stream and the dead zone, $\Delta U = U - U_M$ (Ghisalberti and Nepf 2005), and the width of the layer. Assuming zero net streamwise flow in the dead zone and considering that the thickness of the plane mixing layer is constrained by the width of the dead zone perpendicular to the flow, $W$ (Fig. 1), it follows that

$$b = b_{ideal} = \frac{kU}{W} \tag{2}$$

where $k$ is a dimensionless coefficient, referred to as an "entrainment coefficient" (Valentine and Wood 1977; Weitbrecht et al. 2008) following Taylor's entrainment hypothesis (p.366, Fischer et al. 1979). Although $k$ is often assumed constant as a first approximation (or for particular conditions), it is known to depend on various parameters related to the flow regime and bounding geometry (p. 371, Fischer et al. 1979; Drost, 2012). In the case of transverse mixing between a main stream and a peripheral dead zone of finite depth (i.e. a real mixing layer), the formation of large scale vortices (which controls the rate of exchange) is dependent on the limiting water depth (Weitbrecht et al. 2008). Using mass conservation principles, Weitbrecht et al. (2008) showed that in such cases, the exchange coefficient is given by the dead zone model as

$$b = \frac{kU}{W}\frac{h_E}{h_M} \tag{3}$$

where $h_E$ is the depth at the entrance to the dead zone and $h_M$ is the average depth in the dead zone, as illustrated in Fig. 1. Thus, by determining the coefficient $k$, shear-driven exchange between the main stream and a side-embayment and the associated mean residence times can be evaluated. For tidal flows, $U = U(t)$. Here, we make the assumption that (3) holds approximately for $U = U_{rms}$, implying quasi-steady state conditions.

Valentine and Wood (1977) considered a value of $k = 0.02$ to be generally appropriate for a rectangular cavity in a channel bed, consistent with previous experiments for side cavities. For a range of groyne field geometries and configurations, Weitbrecht et al. (2008) determined via experiments entrainment coefficients ranging from 0.012 to 0.051. They developed an empirical relationship between $k$ and the dead zone geometry, through a nondimensional shape parameter that is fundamentally analogous to a hydraulic radius:

$$R_D = \frac{WL}{h_S(W+L)} \tag{4}$$

where $L$ is the length of the dead zone and $h_S$ is the flow depth in the main stream (Fig. 1). Weitbrecht et al. (2008) contend that the formation of large scale vortices (which controls the rate of exchange) is dependent on the stability of the mixing layer governed by the ratio of the width ($\sim L, W$) to the water depth in the channel ($h_S$). In the specific case of a marina, with one or more breakwaters partially protruding across the entrance (Fig. 1), we argue that the length scales controlling the development of vortices are the entrance width, $L_E$, the smallest depth (usually $h_M$ due to navigational considerations) and $W$. Thus, we propose a modified shape parameter:

$$R_{DM} = \frac{WL_E}{\min(h_M, h_E, h_S)\cdot(W+L_E)} \tag{5}$$

In this paper, we use numerical hydrodynamic model flume tests to evaluate entrainment coefficients for a range of marina geometries and entrance flow conditions. We then apply similar numerical modeling techniques to a number of case studies to investigate the dead zone model's capability to accurately predict residence times in real, micro-tidal marinas and therefore support layout design / optimization.

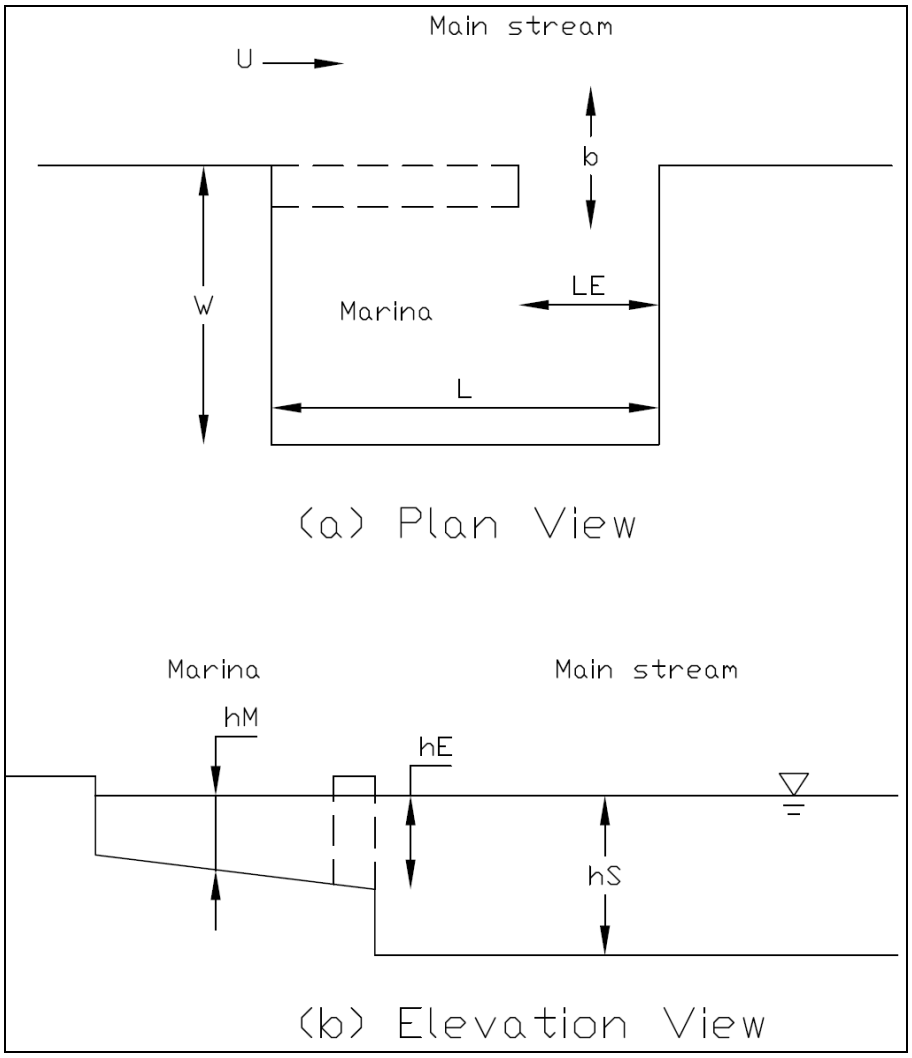


**Figure 1. Schematic of the idealized marina geometry.**

## METHODOLOGY

### Numerical Flume Simulations

A series of systematic numerical flume simulations were implemented to evaluate exchange coefficients for different marina aspect ratios, entrance widths and temporally varying (tidal) flow conditions. The triangular computational meshes of the TELEMAC-2D (Hervouet 2007) models were constructed using the Blue Kenue™ software tool (Canadian Hydraulics Center 2010). Each model mesh consisted of approximately 12,000 triangular elements, with increased resolution at the entrance to the marina and within the basin (characteristic element edge lengths of 10m). The general layout of the computational mesh is shown in Fig. 2 for one of the tests. The open boundary was forced by a sinusoidally varying free surface elevation (12.5h period), to generate oscillating flows along a 20km long x 3km wide channel leading to an artificial "reservoir". The marina was situated midway along one side of the channel. The marina aspect ratio ( $L/W$ ) and the length of the breakwater extending across the entrance ( $L - L_E$ ) were varied systematically to investigate the effects of changes in the marina geometry on flushing rates. The amplitude ( $a = H/2$ ) of the forcing "tidal" signal was also varied in the range 0.125 to 0.75. Details of the forty eight scenarios investigated are listed in Table 1.

Flushing was assessed by simulating the instantaneous release of a conservative (i.e. neutrally buoyant, non-reactive) tracer throughout the marina basin. The tracer was introduced to the numerical model after a "spin-up" period of 6 tidal cycles and assigned an arbitrary initial value of 100 everywhere within the marina basin. The hydrodynamic model was then used to simulate the advection and dispersion of the tracer over a 15-day period, to quantify the exchange between the marina and the main channel.

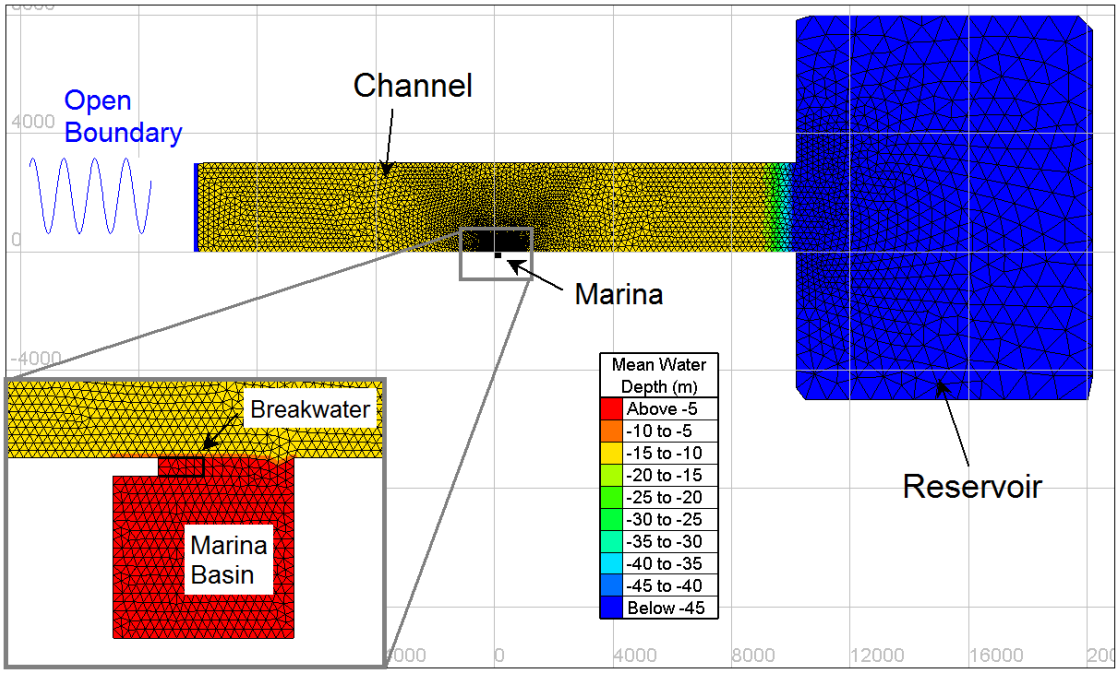


**Figure 2. Numerical flume domain, bathymetry and computational mesh.**

**Table 1. Summary of parameters for the numerical flume simulations.**

| Run | $L_E$ (m) | $L$ (m) | $W$ (m) | $h_E$ (m) | $h_M$ (m) | $h_S$ (m) | $H$ (m) | $Re = U_{rms}h_S / \nu$ |
|---|---|---|---|---|---|---|---|---|
| 001 | 200 | 200 | 200 | 5 | 5 | 15 | 1.0 | 300 |
| 002 | 150 | 200 | 200 | 5 | 5 | 15 | 1.0 | 300 |
| 003 | 100 | 200 | 200 | 5 | 5 | 15 | 1.0 | 300 |
| 004 | 50 | 200 | 200 | 5 | 5 | 15 | 1.0 | 300 |
| 005 | 200 | 200 | 150 | 5 | 5 | 15 | 1.0 | 300 |
| 006 | 150 | 200 | 150 | 5 | 5 | 15 | 1.0 | 300 |
| 007 | 100 | 200 | 150 | 5 | 5 | 15 | 1.0 | 300 |
| 008 | 50 | 200 | 150 | 5 | 5 | 15 | 1.0 | 300 |
| 009 | 200 | 200 | 100 | 5 | 5 | 15 | 1.0 | 300 |
| 010 | 150 | 200 | 100 | 5 | 5 | 15 | 1.0 | 300 |
| 011 | 100 | 200 | 100 | 5 | 5 | 15 | 1.0 | 300 |
| 012 | 50 | 200 | 100 | 5 | 5 | 15 | 1.0 | 300 |
| 013 | 200 | 200 | 200 | 5 | 5 | 15 | 0.5 | 150 |
| 014 | 150 | 200 | 200 | 5 | 5 | 15 | 0.5 | 150 |
| 015 | 100 | 200 | 200 | 5 | 5 | 15 | 0.5 | 150 |
| 016 | 50 | 200 | 200 | 5 | 5 | 15 | 0.5 | 150 |
| 017 | 200 | 200 | 150 | 5 | 5 | 15 | 0.5 | 150 |
| 018 | 150 | 200 | 150 | 5 | 5 | 15 | 0.5 | 150 |
| 019 | 100 | 200 | 150 | 5 | 5 | 15 | 0.5 | 150 |
| 020 | 50 | 200 | 150 | 5 | 5 | 15 | 0.5 | 150 |
| 021 | 200 | 200 | 100 | 5 | 5 | 15 | 0.5 | 150 |
| 022 | 150 | 200 | 100 | 5 | 5 | 15 | 0.5 | 150 |
| 023 | 100 | 200 | 100 | 5 | 5 | 15 | 0.5 | 150 |
| 024 | 50 | 200 | 100 | 5 | 5 | 15 | 0.5 | 150 |
| 025 | 200 | 200 | 200 | 5 | 5 | 15 | 0.25 | 80 |
| 026 | 150 | 200 | 200 | 5 | 5 | 15 | 0.25 | 80 |
| 027 | 100 | 200 | 200 | 5 | 5 | 15 | 0.25 | 80 |
| 028 | 50 | 200 | 200 | 5 | 5 | 15 | 0.25 | 80 |
| 029 | 200 | 200 | 150 | 5 | 5 | 15 | 0.25 | 80 |
| 030 | 150 | 200 | 150 | 5 | 5 | 15 | 0.25 | 80 |
| 031 | 100 | 200 | 150 | 5 | 5 | 15 | 0.25 | 80 |
| 032 | 50 | 200 | 150 | 5 | 5 | 15 | 0.25 | 80 |
| 033 | 200 | 200 | 100 | 5 | 5 | 15 | 0.25 | 80 |
| 034 | 150 | 200 | 100 | 5 | 5 | 15 | 0.25 | 80 |
| 035 | 100 | 200 | 100 | 5 | 5 | 15 | 0.25 | 80 |
| 036 | 50 | 200 | 100 | 5 | 5 | 15 | 0.25 | 80 |
| 037 | 200 | 200 | 200 | 5 | 5 | 15 | 1.5 | 480 |
| 038 | 150 | 200 | 200 | 5 | 5 | 15 | 1.5 | 480 |
| 039 | 100 | 200 | 200 | 5 | 5 | 15 | 1.5 | 480 |
| 040 | 50 | 200 | 200 | 5 | 5 | 15 | 1.5 | 480 |
| 041 | 200 | 200 | 150 | 5 | 5 | 15 | 1.5 | 480 |
| 042 | 150 | 200 | 150 | 5 | 5 | 15 | 1.5 | 480 |
| 043 | 100 | 200 | 150 | 5 | 5 | 15 | 1.5 | 480 |
| 044 | 50 | 200 | 150 | 5 | 5 | 15 | 1.5 | 480 |
| 045 | 200 | 200 | 100 | 5 | 5 | 15 | 1.5 | 480 |
| 046 | 150 | 200 | 100 | 5 | 5 | 15 | 1.5 | 480 |
| 047 | 100 | 200 | 100 | 5 | 5 | 15 | 1.5 | 480 |
| 048 | 50 | 200 | 100 | 5 | 5 | 15 | 1.5 | 480 |

## Case Studies

The systematic numerical flume simulations described in the preceding section were designed to determine empirical relationships between water exchange, flow characteristics and geometry for idealized marina geometries (i.e. rectangular) and hydrodynamic conditions. However, the ultimate goal is to develop a pragmatic methodology for evaluating residence times in real micro-tidal marinas. A series of numerical modeling case studies, incorporating field measurements of currents and water levels, were therefore implemented to evaluate the effectiveness of the dead zone model for practical applications.

The computational domains of the numerical models were set up to reflect available boundary condition data and the locations of the marina sites. The coastlines and bathymetries of the models were generated from:

- Detailed topographic and bathymetric surveys of the sites and adjacent areas;
- Digitized geo-referenced satellite images;
- Geo-referenced drawings of the marina layouts.

The hydrodynamic models were calibrated and validated against field measurements of water levels (tide gauge data) and currents (acoustic Doppler current profiler data). The tidal regimes at the sites ranged from mixed diurnal / semi-diurnal to predominantly semi-diurnal, with tidal prism ratios ($TPR = \overline{H} / h_M$, where the overbar denotes a temporal mean) ranging from 0.05 to 0.6 (Table 2). No field survey data, such as tracer or drogue studies, was available to facilitate calibration and / or validation of the dispersion coefficients applied.

Flushing was assessed in the same way as for the numerical flume runs, by releasing a conservative tracer in the marina basin and tracking the concentration of the tracer over time. The tracer was released during neap tide conditions as this typically provides the most conservative time estimate of tide-driven water exchange.

Details of the twenty case study simulations are listed in Table 2. As many of the marinas were irregularly shaped (Fig. 3), the principal orthogonal dimensions ($L$ and $W$) were estimated as objectively as possible by first selecting the most apparent clear dimension and then dividing this into the marina area. For marinas with multiple entrances, $L_E$ was determined based on the total (combined) entrance width.

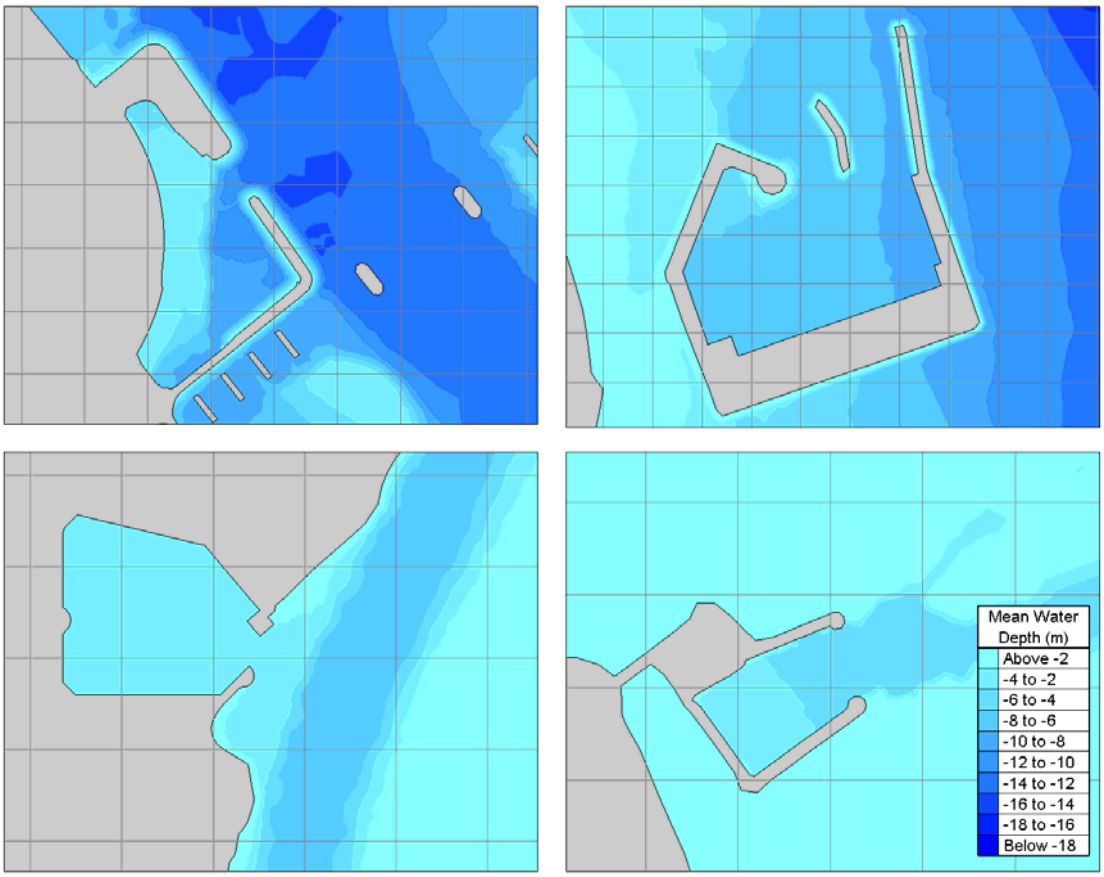


**Figure 3. Example marina case study layouts (rectangular grids are shown at 100m x 100m resolution to indicate scale).**

**Table 2. Summary of parameters for the case study simulations.**

| Run | $L_E$ (m) | $L$ (m) | $W$ (m) | $h_E$ (m) | $h_M$ (m) | $h_S$ (m) | $H$ (m) | $Re = U_{rms}h_S / \nu$ |
|---|---|---|---|---|---|---|---|---|
| SYT1 | 35 | 160 | 215 | 3.2 | 3.2 | 7.0 | 1.0 | 70 |
| SYT2 | 35 | 160 | 215 | 3.2 | 2.9 | 7.0 | 1.0 | 70 |
| SYT3 | 77 | 160 | 215 | 3.2 | 3.2 | 7.0 | 1.0 | 70 |
| SYT4 | 56 | 160 | 215 | 3.2 | 3.2 | 7.0 | 1.0 | 70 |
| KUT1 | 275 | 450 | 425 | 6.5 | 8.5 | 8.5 | 1.6 | 45 |
| KUT2 | 360 | 375 | 950 | 11.3 | 8.7 | 15.5 | 1.7 | 310 |
| KUT3 | 235 | 740 | 1300 | 13.0 | 13.0 | 14.0 | 1.7 | 420 |
| BTN1 | 22 | 50 | 60 | 3.6 | 4.5 | 3.8 | 0.6 | 7.7 |
| BTN2 | 22 | 50 | 60 | 3.6 | 4.5 | 3.8 | 1.0 | 8.9 |
| BTN3 | 22 | 50 | 60 | 3.6 | 4.5 | 3.8 | 1.4 | 9.8 |
| BTN4 | 22 | 50 | 60 | 3.6 | 4.5 | 3.8 | 1.7 | 10.6 |
| BTN5 | 22 | 50 | 60 | 3.6 | 4.5 | 3.8 | 2.1 | 11.2 |
| ZKA1 | 75 | 105 | 160 | 4.5 | 3.5 | 5.3 | 0.6 | 12.3 |
| ZKA2 | 75 | 105 | 160 | 4.5 | 3.5 | 5.3 | 1.0 | 30 |
| ZKA3 | 75 | 105 | 160 | 4.5 | 3.5 | 5.3 | 1.4 | 45 |
| ZKA4 | 75 | 105 | 160 | 4.5 | 3.5 | 5.3 | 1.7 | 60 |
| ZKA5 | 75 | 105 | 160 | 4.5 | 3.5 | 5.3 | 2.1 | 70 |
| KBM1 | 80 | 390 | 160 | 7.0 | 6.1 | 12.2 | 1.1 | 370 |
| QBP1 | 165 | 760 | 450 | 6.7 | 7.1 | 5.7 | 0.4 | 14.2 |
| QBP2 | 165 | 760 | 450 | 6.6 | 7.0 | 5.5 | 0.4 | 14.8 |

## RESULTS AND DISCUSSION

### Numerical Flume Tests

Results for each of the systematic numerical flume simulations are listed in Table 3. Fig. 4 shows the basin-averaged relative tracer concentration, $C / C_0$, versus time (normalized by the semi-diurnal period, $T_P = 12.5$h) for Run 003. The exchange coefficient, $b$, was evaluated from a least squares exponential fit to the basin-averaged tracer concentration (e.g., Seo and Cheong 2001). Plotted on a logarithmic scale, the mean tracer concentration in the marina appears linear for two separate, distinct phases ($t < 2T_P$ and $t > 6T_P$). In the initial phase, flushing of the marina is rapid, as indicated by a best fit exchange coefficient $b_0 = 1.5 \times 10^{-5}$ s$^{-1}$. After approximately six tidal periods, diminished concentration gradients and enhanced return flows lead to significantly slower exchange ($b_1 = 7.8 \times 10^{-7}$ s$^{-1}$). The trend was consistent across all runs, suggesting that mass exchange between the marina and the channel is not strictly a first order process. This corroborates the findings of previous field and numerical studies of mass exchange in groyne fields (cited by McCoy 2006). In particular, the marina is not well mixed in the initial phase, as indicated by strong tracer concentration gradients (Fig. 5). This suggests that a multi-region dead zone model (Drost 2012) may provide a more accurate representation of mixing processes for micro-tidal marinas. Nevertheless, the overall best fit first order exchange coefficient provides a consistent basis for comparing time scales of water renewal in the marina.

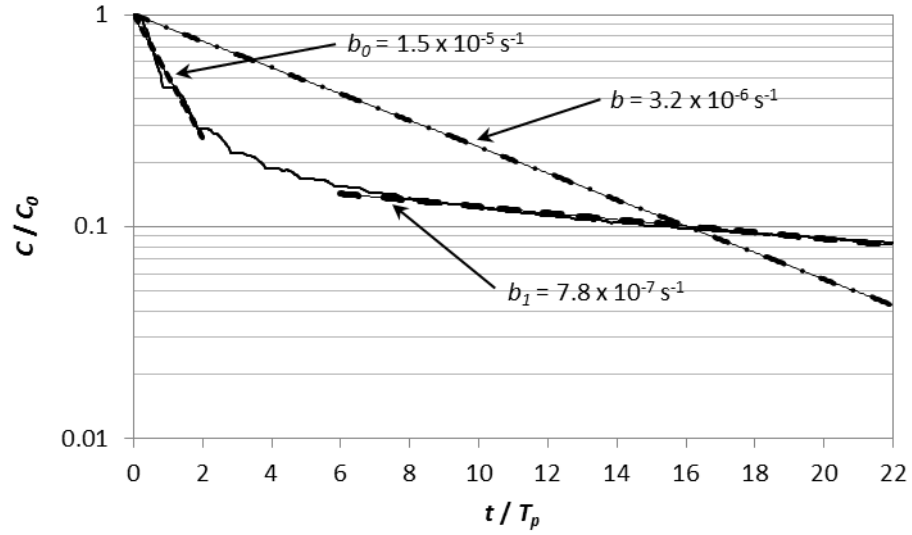


**Figure 4. Normalized marina-averaged tracer concentration (solid line) and first order exchange coefficient fits (dashed lines) for Run 003.**

**Table 3. Summary of numerical flume test results.**

| Run | $b$ x $10^6$ ($s^{-1}$) | $T_R$ (days) | $k$ x $10^3$ (-) | | Run | $b$ x $10^6$ ($s^{-1}$) | $T_R$ (days) | $k$ x $10^3$ (-) |
|---|---|---|---|---|---|---|---|---|
| 001 | 5.0 | 2.3 | 4.97 | | 025 | 4.2 | 2.7 | 1.56 |
| 002 | 3.7 | 3.2 | 3.65 | | 026 | 3.4 | 3.4 | 1.24 |
| 003 | 3.2 | 3.6 | 3.19 | | 027 | 2.6 | 4.5 | 9.52 |
| 004 | 2.7 | 4.3 | 2.67 | | 028 | 1.5 | 7.8 | 5.53 |
| 005 | 5.5 | 2.1 | 4.12 | | 029 | 4.8 | 2.4 | 1.33 |
| 006 | 4.1 | 2.8 | 3.06 | | 030 | 3.8 | 3.0 | 10.58 |
| 007 | 3.5 | 3.4 | 2.59 | | 031 | 3.0 | 3.9 | 8.30 |
| 008 | 2.8 | 4.1 | 2.11 | | 032 | 1.6 | 7.3 | 4.41 |
| 009 | 5.8 | 2.0 | 2.88 | | 033 | 5.6 | 2.1 | 10.29 |
| 010 | 4.9 | 2.4 | 2.46 | | 034 | 4.5 | 2.6 | 8.34 |
| 011 | 4.1 | 2.9 | 2.03 | | 035 | 3.6 | 3.3 | 6.58 |
| 012 | 3.0 | 3.9 | 1.49 | | 036 | 1.1 | 10.3 | 2.08 |
| 013 | 4.4 | 2.6 | 8.87 | | 037 | 5.0 | 2.3 | 3.10 |
| 014 | 3.4 | 3.4 | 6.83 | | 038 | 3.7 | 3.1 | 2.30 |
| 015 | 2.8 | 4.1 | 5.67 | | 039 | 3.1 | 3.7 | 1.95 |
| 016 | 2.2 | 5.2 | 4.42 | | 040 | 2.8 | 4.1 | 1.77 |
| 017 | 5.2 | 2.2 | 7.78 | | 041 | 5.2 | 2.2 | 2.45 |
| 018 | 3.9 | 2.9 | 5.90 | | 042 | 4.0 | 2.9 | 1.87 |
| 019 | 3.2 | 3.6 | 4.86 | | 043 | 3.3 | 3.5 | 1.56 |
| 020 | 2.4 | 4.9 | 3.52 | | 044 | 2.9 | 4.0 | 1.37 |
| 021 | 5.8 | 2.0 | 5.85 | | 045 | 5.3 | 2.2 | 1.65 |
| 022 | 4.8 | 2.4 | 4.82 | | 046 | 4.6 | 2.5 | 1.45 |
| 023 | 4.1 | 2.8 | 4.06 | | 047 | 3.8 | 3.1 | 1.18 |
| 024 | 1.6 | 7.2 | 1.61 | | 048 | 3.0 | 3.9 | 0.93 |

The formation of large scale vortices at the interface between the marina and the main channel was evident for all numerical flume simulations, as shown in Fig. 5 for Runs 001 and 002. This suggests shear-generated circulation is the dominant exchange mechanism. The scale and efficiency (in terms of driving water exchange) of the vortices increased with entrance cross-sectional area, confirming:

1. $L_E$ is an appropriate choice of length scale for (5); and
2. Entrance area guidelines developed for tide-dominated exchange (Cox et al. 2008) are not applicable under these conditions.

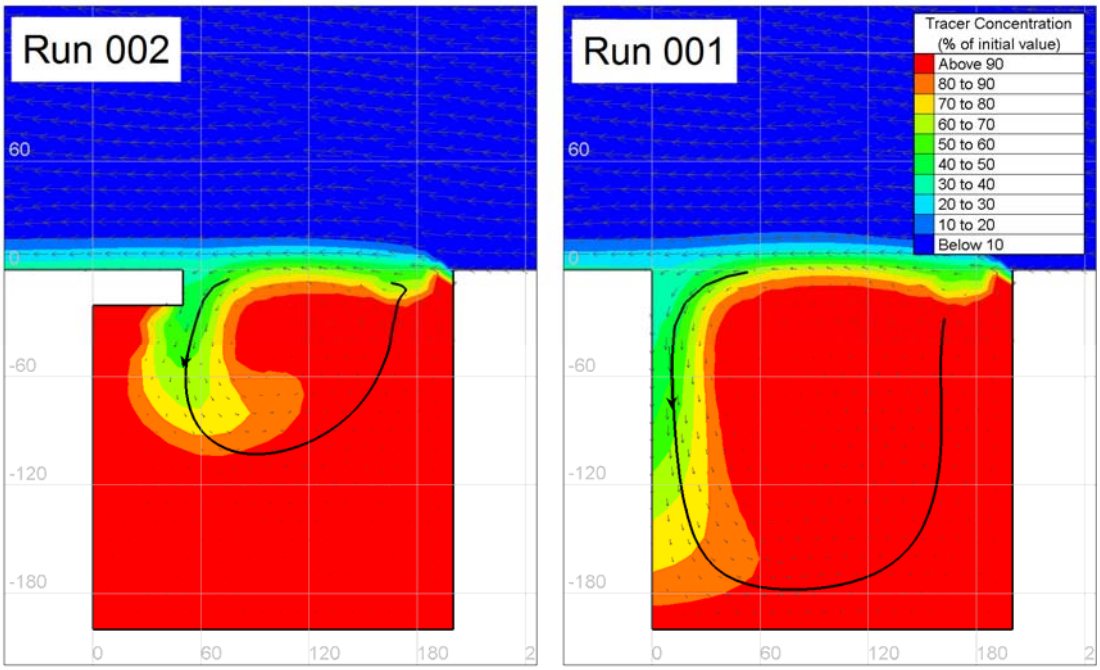


**Figure 5. Tracer concentrations and velocity vectors for Runs 001 (right) and 002 (left), 2.5h following release of the tracer.**

Fig. 6 shows the entrainment coefficient, $k$, determined from (3) and the best fit $b$ for each numerical flume simulation, plotted against the modified shape parameter in (5). For a given set of tidal conditions and channel depth-based Reynolds numbers ($\mathrm{Re} = U_{rms} h_S / \nu$), there is statistically significant ($\alpha = 0.05$) correlation between $k$ and $R_{DM}$, suggesting the dead zone model and the length scales adopted in the modified shape parameter are generally valid. By contrast, there is no apparent correlation between $k$ and the groyne field shape parameter, $R_D$ (Fig. 7), demonstrating the importance of the entrance width in controlling exchange. The tidal prism ratio (Fig. 8), relative marina entrance area ($A/a$, where $A = LW$ and $a = L_E h_E$, Fig. 9) and other traditional indicators for tide-driven exchange (Cox et al. 2008) do not provide consistent predictors of residence times for the cases investigated. Interestingly, entrainment coefficients begin to converge for tidal prism ratios around 0.3 (i.e. for the highest Reynolds numbers investigated), suggesting $R_{DM}$ is not a useful indicator of optimal marina geometry for $TPR \geq 0.3$ (Fig. 10). This falls within the range of threshold minimum tidal prism ratios (0.25 to 0.35) recommended by Cox et al. (2008) to ensure "good flushing" based on purely tide-driven exchange principles.

It is not clear why $k$ decreases with increasing Reynolds number, although a visual comparison of velocity vectors and tracer concentrations suggests that this may be related to a dominance of "sweeps" (momentum inflows) and a suppression of "ejection" (momentum outflow) events at higher Reynolds numbers leading to less efficient exchange. On a purely empirical basis, $k = 0.06 R_{DM} / \mathrm{Re}$ provides a good fit to the data and emphasises the reducing dependence of $k$ on $R_{DM}$ for higher Reynolds numbers. However, due to the limited channel and marina depth configurations investigated, further work is necessary to confirm this relationship holds for the full range of typical field conditions.

The computed values of $k$ are generally lower than the ranges determined experimentally by Valentine and Wood (1977) and Weitbrecht et al. (2008) for steady flows. This is simply related to the choice of $U_{rms}$ as the velocity scale for use in the dead zone model for unsteady flows, rather than any physical phenomenon. However, observations have shown that mass transfer rates for oscillatory flows may be significantly different to those for comparable unidirectional currents (Lowe et al. 2005).

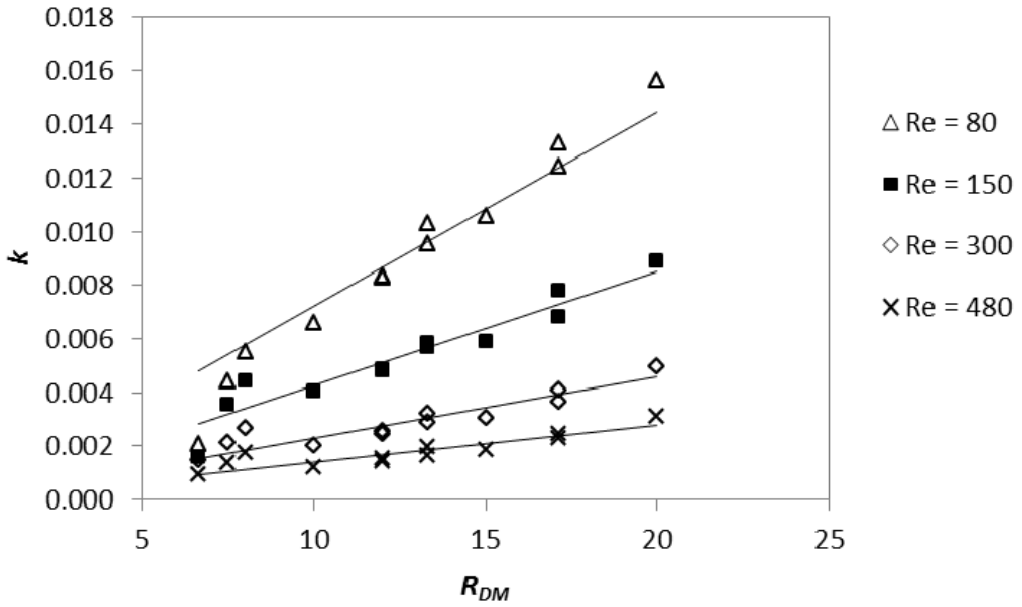


**Figure 6. Entrainment coefficient as a function of the modified shape parameter.**

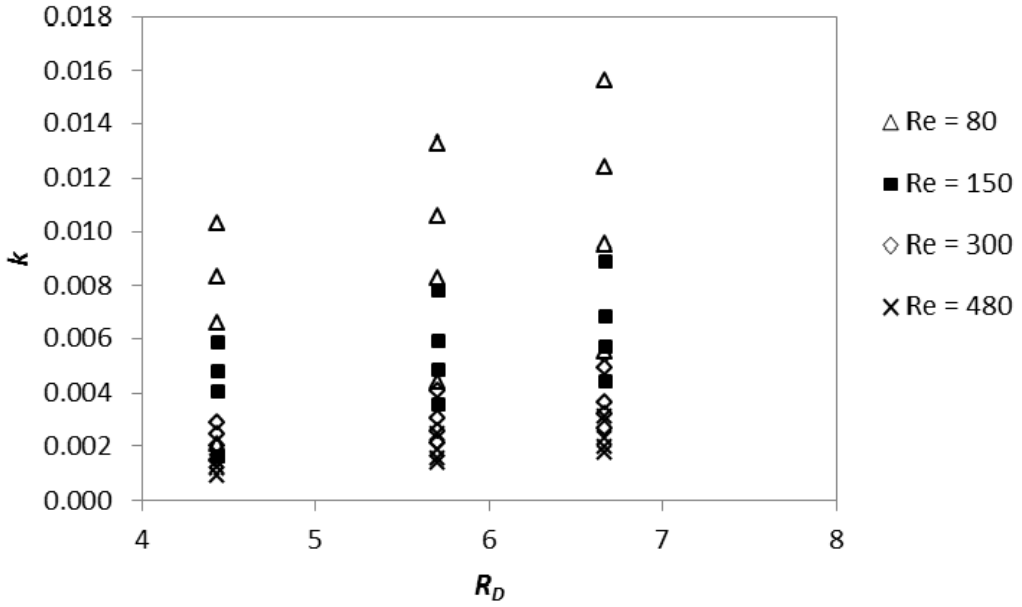


**Figure 7. Entrainment coefficient versus groyne field shape parameter (Weitbrecht et al. 2008).**

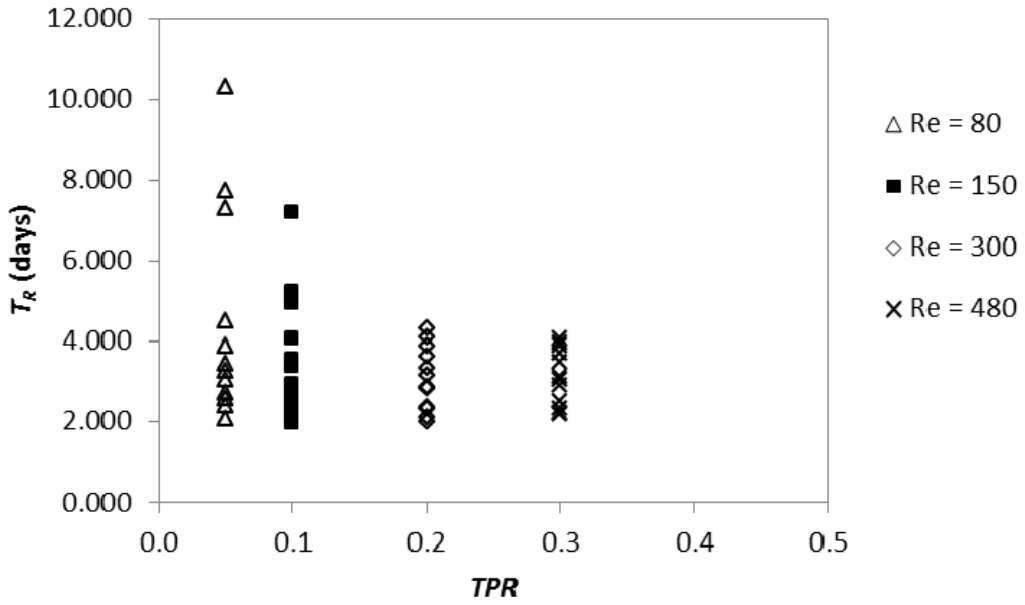


**Figure 8. Marina mean residence time versus tidal prism ratio.**

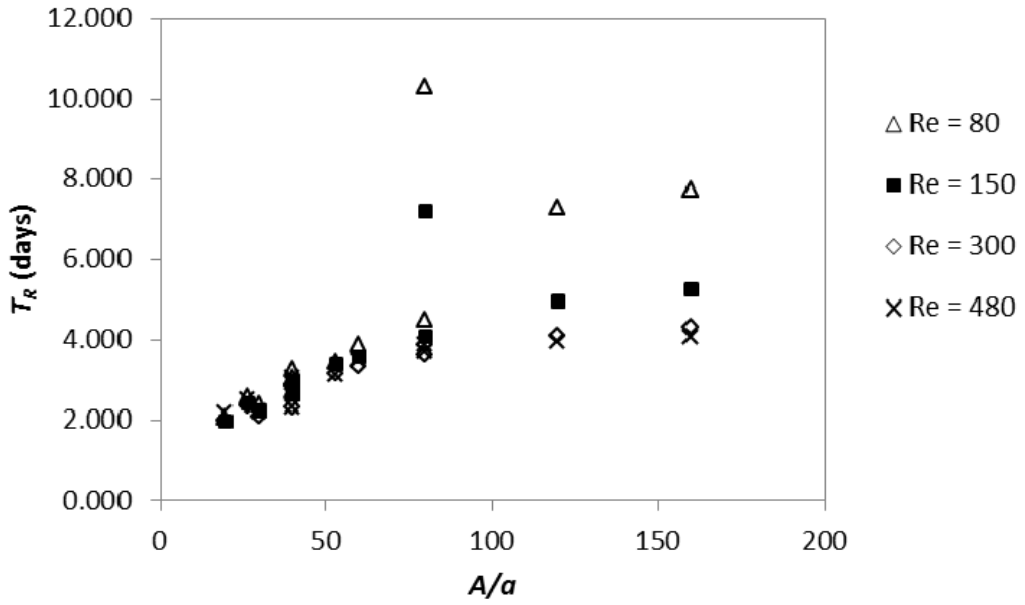


**Figure 9. Marina mean residence time versus relative marina entrance area.**

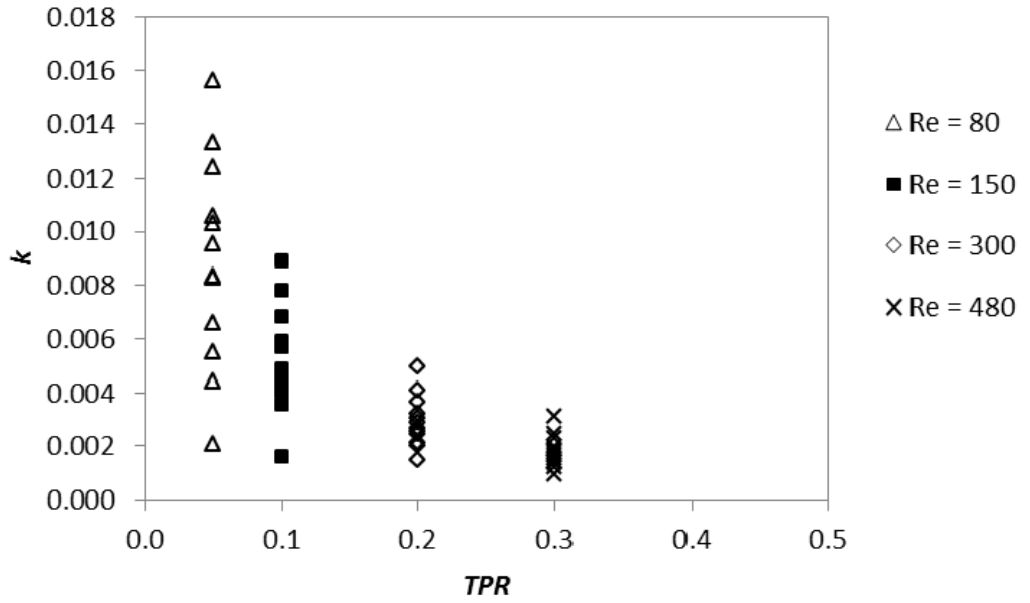


**Figure 10. Entrainment coefficient versus tidal prism ratio.**

## Case Studies

First order exchange coefficients and residence times for the marina case studies, obtained directly from exponential fits to computed time series basin-averaged tracer concentrations, are listed in Table 4.

The results of the numerical flume simulations suggest that, if the marina geometry and external flow characteristics are known *a priori*, the mean residence time can be evaluated for tidal prism ratios up to about 0.3. To test this inference, mean residence times obtained by the "direct" method described above were compared to residence times predicted using the dead zone model (Fig. 11). Best fit $k$ values from the numerical flume studies were linearly interpolated according to $\mathrm{Re}$ for each case study. There is significant correlation ($\alpha = 0.05$) between residence times obtained directly from the numerical models and based on the dead zone model. Even for irregular marina geometries (some including multiple entrances), mixed diurnal and semi-diurnal tides, and tidal prism ratios exceeding 0.3 (i.e. not necessarily micro-tidal), the dead zone model appears to provide reasonable estimates of mean residence time.

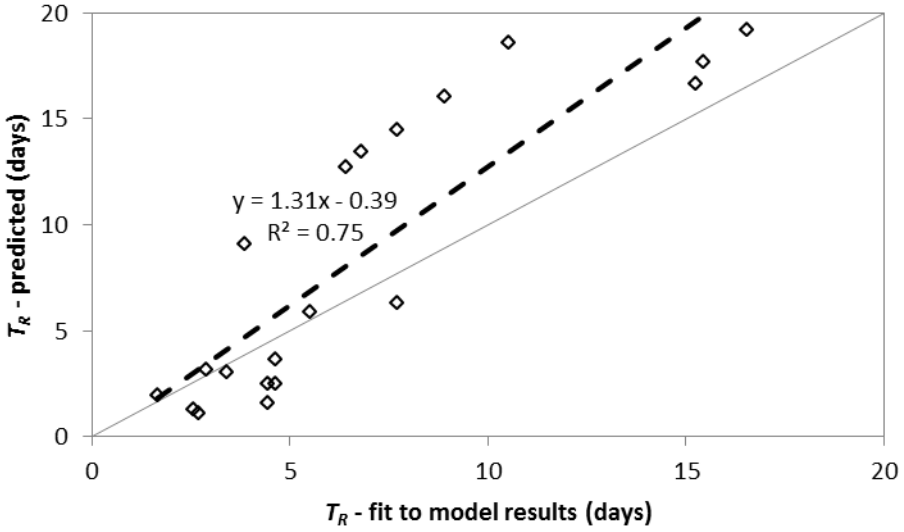


**Figure 11. Marina mean residence times from numerical model results and the dead zone model.**

**Table 4. Summary of results for case studies.**

| Run | $b$ x $10^6$ ($s^{-1}$) | $T_R$ (days) |
|---|---|---|
| SYT1 | 2.5 | 4.8 |
| SYT2 | 3.4 | 3.4 |
| SYT3 | 7.0 | 1.7 |
| SYT4 | 2.6 | 4.3 |
| KUT1 | 3.0 | 3.9 |
| KUT2 | 1.5 | 7.7 |
| KUT3 | 0.7 | 16.5 |
| BTN1 | 1.1 | 10.4 |
| BTN2 | 1.3 | 8.9 |
| BTN3 | 1.5 | 7.9 |
| BTN4 | 1.7 | 7.0 |
| BTN5 | 1.8 | 6.3 |
| ZKA1 | 2.1 | 5.6 |
| ZKA2 | 2.5 | 4.6 |
| ZKA3 | 2.6 | 4.5 |
| ZKA4 | 4.5 | 2.6 |
| ZKA5 | 4.3 | 2.7 |
| KBM1 | 4.0 | 2.9 |
| QBP1 | 0.8 | 15.4 |
| QBP2 | 0.8 | 15.4 |

## CONCLUSION

A series of numerical hydrodynamic model flume tests and case studies were used to extend the dead zone model, traditionally used to assess water exchange between river channels and quasi-stagnant peripheral zones, to micro-tidal marinas. For tidal prism ratios less than about 0.3, the dead zone model provides a better means to guide optimization of marina and entrance geometry than methods developed for tide-driven exchange. For the limited range of conditions investigated, $TPR \approx 0.3$ represents a point of transition from shear- to tide-driven exchange.

Further research and additional field data is needed to validate the dead zone model for a more comprehensive range of water depths and relative marina depths, and to explore the dependency on Reynolds number and intrinsic mixing parameters (e.g. dispersion coefficients applied in the numerical models).

The dead zone model presented here assumes mass exchange between marinas and adjacent waters can be reasonably approximated by a first order process. The results of numerical simulations indicated that this is not strictly valid and the model could potentially be improved by considering higher order exchange processes (e.g. involving multi-zone models). Alternatives to the mean residence time that take into account distinct phases of mass exchange may therefore provide more appropriate indicators of water renewal to support assessments of water quality, depending on the relative time scales of biochemical processes being considered.

## ACKNOWLEDGEMENTS

James Walker is gratefully acknowledged for his useful technical comments. The authors thank Jack Bokaris for obtaining permission to use the case study materials presented herein. Enda Murphy is grateful to Jorge Trindade for supporting his attendance at ICCE2012 and Heidi Nepf for providing useful references.

## REFERENCES

Atkinson, T.C., and P.M. Davis. 2000. Longitudinal dispersion in natural channels: 1. Experimental results from the River Severn, U.K., *Hydrol. and Earth Sys. Sci.*, 4, 345-353.

Bencala, K.E., and R.A. Walters. 1983. Simulation of solute transport in a mountain pool-and-riffle stream: A transient storage model, *Water Resour. Res.*, 19, 3, 718-724.

Barber, R.W., and M.J. Wearing. 2002. A mathematical model for predicting the pollution exchange coefficient of small tidal embayments, *Proc. Int. Conf. Protection and Restoration of the Environment VI*, 355-362.

Canadian Hydraulics Centre, National Research Council. 2010. Blue Kenue™ Reference Manual.

Chikwendu, S.C., and G.U. Ojiakor. 1985. Slow-zone model for longitudinal dispersion in two-dimensional shear flows, *J. Fluid Mech.*, 152, 15-38.

Cox, J.C., H.N. Smith, A.F. Nielsen, M.A. Pirrello, S. Desloovere, C. Mead, and A. van Tonder. 2008. Protecting water quality in marinas, *Report of International Working Group 98,* convened by the

Recreational Navigation Commission, Permanent International Association of Navigational Congresses.

Davis, P.M., T.C. Atkinson, and T.M.L. Wigley. 2000. Longitudinal dispersion in natural channels: 2. The roles of shear flow dispersion and dead zones in the River Severn, U.K., *Hydrol. and Earth Sys. Sci.*, 4, 355-371.

Davis, P.M., and T.C. Atkinson. 2000. Longitudinal dispersion in natural channels: 3. An aggregated dead zone model applied to the River Severn, U.K., *Hydrol. and Earth Sys. Sci.*, 4, 373-381.

Drost, K.J. 2012. RANS and LES predictions of turbulent scalar transport in dead zones of natural streams. MSc dissertation, Oregon State University.

Fischer, H.B., E.J. List, R.C.Y. Koh, J. Imberger, and N.H. Brooks. 1979. *Mixing in Inland and Coastal Waters*, Academic Press, London, 483 pp.

Ghisalberti, M., and H.M. Nepf. 2002. Mixing layers and coherent structures in vegetated aquatic flows, *J. Geophys. Res.*, 107, C2, 1-11.

Ghisalberti, M., and H. Nepf. 2005. Mass transport in vegetated shear flows, *Env. Fluid Mech.*, 5, 527-551.

Harvey, J.W., B.J. Wagner, and K.E. Bencala. 1996. Evaluating the reliability of the stream tracer approach to characterize stream-subsurface water exchange, *Water Resour. Res.*, 32, 2441-2451.

Harvey, J.W., J.E. Saiers, and J.T. Newlin. 2005. Solute transport and storage mechanisms in wetlands of the Everglades, south Florida, *Water Resour. Res.*, 41, 1-14.

Hervouet, J.M. 2007. *Hydrodynamics of Free Surface Flows: Modelling with the Finite Element Method*, John Wiley & Sons, Chichester, West Sussex, 341 pp.

Kundu, P.K., and I.M. Cohen. 2004. *Fluid Mechanics*, 3rd ed., Elsevier Academic Press, San Diego, California, 759 pp.

Lowe, R.J., J.R. Koseff, and S.G. Monismith. 2005. Oscillatory flow through submerged canopies: 2. Canopy mass transfer, *J. Geophys. Res.*, 110, 1-14.

McCoy, A.M. 2006. Numerical investigations using LES: exploring flow physics and mass exchange near groynes. Ph.D dissertation, University of Iowa.

Monsen, N.E., J.E. Cloern, L.V. Lucas, and S.G. Monismith. 2002. A comment on the use of flushing time, residence time, and age as transport time scales, *Limnol. Oceanogr.*, 47, 5, 1545-1553.

Murphy, E., and J. Walker. 2011. Shear-driven flushing and circulation in a marina in the United Arab Emirates, *Proc. XVIIIth Telemac & Mascaret User Club Conf.*, Chatou., 77-85.

Nepf, H., M. Ghisalberti, B. White, and E. Murphy. 2007. Retention time and dispersion associated with submerged aquatic canopies, *Water Resour. Res.*, 43, 1-10.

Nielsen, A.F., and A.D. McCowan. 1994. A natural flushing system for artificial harbours: a case study of the Anchorage Port Stephens, Corlette, N.S.W., *Trans. Multi-Disc. Eng.*, GE18, 41-48.

Pugh, D.T. 1987. *Tides, Surges and Mean Sea-Level.* John Wiley & Sons, London, 472 pp.

Purnama, A. 1988. The effect of dead zones on longitudinal dispersion in streams, *J. Fluid Mech.*, 186, 351-377.

Rafferty, J.P. (Ed.) 2012. *Landforms*, 1st ed., Britannica Educational Publishing, New York, 273 pp.

Raupach, M.R., J.J. Finnigan, and Y. Brunet. 1996. Coherent eddies and turbulence in vegetation canopies: The mixing layer analogy, *Boun. Layer Meteor.*, 78, 351-382.

Riviere, N., M. Garcia, E. Mignot, and G. Travin. 2010. Characteristics of the recirculation cell pattern in a lateral cavity, *Proc. Int. Conf. Fluvial Hydraul.*, IAHR, 673-679.

Schmid, B.H. 2002. Persistence of skewness in longitudinal dispersion data: can the dead zone model explain it after all?, *J. Hydraul. Eng.*, 128, 848-854.

Seo, I.W., and T.S. Cheong. 2001. Moment-based calculation of parameters for the storage zone model for river dispersion, *J. Hydraul. Eng.*, 127(6), 453-465.

U.S.E.P.A. 1985. Coastal Marinas Assessment Handbook, EPA 904/6-85-132.

U.S.E.P.A. 2001. National Management Measures Guidance to Control Nonpoint Source Pollution from Marinas and Recreational Boating, EPA 841-B-01-005.

Valentine, E.M., and I.R. Wood. 1977. Longitudinal dispersion with dead zones, *J. Hydraul. Div.*, 103, 975-989.

van Mazijk, A., and E.J.M. Veling. 2004. Tracer experiments in the Rhine Basin: evaluation of the skewness of observed concentration distributions, *J. Hydrol.*, 307, 60-78.

Weitbrecht, V., S.A. Socolofsky, and G.H. Jirka. 2008. Experiments on mass exchange between groin fields and main stream in rivers, *J. Hydraul. Eng.*, 134, 173-183.

Weitbrecht, V., W. Uijttewaal, and G.H. Jirka. 2004. A random walk approach for investigating near- and far-field transport phenomena in rivers with groin fields, *Proc. River Flow 2004 Conference*, IAHR, Naples, 1-10.

Weitbrecht, V., W. Uijttewaal, and G.H. Jirka. 2003. 2-D particle tracking to determine transport characteristics in rivers with dead zones, In *International Symposium on Shallow Flows*, Delft.

Worman, A. 2000. Comparison of models for transient storage of solutes in small streams, *Water Resour. Res.*, 36, 455-468.